*Int. J. Electrochem. Sci.*, 17 **(2022)** Article Number: 220134, doi: 10.20964/2022.01.38

International Journal of
ELECTROCHEMICAL
SCIENCE
www.electrochemsci.org

*Short Communication*

# Investigation of Metal Coated D32 Steel Corrosion in Marine Environment

*Gang Zhao*[*], *Weihua Zhang and Mingtao Zhao*

Qingdao Huanghai University, Qingdao 266427, China
[*]E-mail: zhao_8097@163.com

*Received:* 30 Sepember 2021 / *Accepted:* 15 November 2021 / *Published:* 6 December 2021

To explore a metal coating suitable for metal corrosion protection in ocean low-salinity dry-wet cycle environment, taking the corrosion environment with low salinity in Bohai Sea area as the research object, the corrosion behavior and pitting characteristic of D32 steel with different metal coatings (Al, Mg, Cu and Zn) with the thickness of 30±1 μm was studied through electrochemical test and corrosion morphology analysis, so as to determine the best protective metal coatings. The results showed that under the condition of 20 dry-wet cycles and low chloride ion concentration, the four samples were in activated conditions and anode controlled. The corrosion potential of four metal coatings was Cu < Zn < Al < Mg-coated steel, the corrosion current density was Zn < Cu < Mg < Al-coated steel, the general corrosion rate was Al < Cu < Zn < Mg-coated steel, and the pitting corrosion rate was Mg < Zn < Cu < Al-coated steel. Therefore, under the research conditions in this paper, Zn coating can be used to protect D32 steel in the ocean spray area with low salinity.

**Keywords:** Low salinity; Wet-dry cycle; Metal coating; D32 steel

## 1. INTRODUCTION

Marine corrosive environment is one of the key factors affecting the life of offshore platforms. The marine corrosion area is divided into five areas: atmospheric area, spray splashing area, tidal range area, full immersion area and marine mud area [1]. The atmospheric area is mainly characterized by atmospheric corrosion, and the corrosion rate is low, about 0.03-0.08 mm/a [2,3]. In the tidal range area, waterline corrosion is mainly manifested, and the corrosion rate is about 0.1-0.37 mm/a [4,5]. The corrosion behavior of metals in full leaching zone and sea mud zone is affected by a series of factors, such as dissolved oxygen, microorganism, pH and organic matter. The corrosion morphology of metals is general corrosion state and corrosion state, and the corrosion rate is about 0.13-0.25 mm/a and 0.02-0.08 mm/a, respectively. The corrosion rate of the splash area is much higher than those of

the above four areas, generally ranging from 0.3 mm/a to 0.5 mm/a and even up to 2.5 mm/a (Alaskikoc Bay).

Due to its location in the interface area of sea-air exchange, the splash area is often in a humid and oxygen-rich state with strong and frequent wave impact [6]. And also the steel structure is in a dry-wet cycle state in the splashing area. In addition, high salt content [7], erosion of sea water, adequate oxygen supply, sufficient sunshine and rising temperature lead to the most serious corrosion of steel structure in the splash area. Zhu et al. [8] used ACM-1512B intelligent atmospheric corrosion monitor to measure the wettability of water film on steel samples in splash area and atmospheric area, and also measured the deposition amount of salt ions. Their research results showed that water film on steel samples in spray area had long wettability time and large current. Moreover, the amount of salt particles near the peak value of the splashing area was much higher than other parts of the splash area. The most serious external causes of corrosion were the long wetting time of seawater film, the high frequency of dry-wet cycles, the accumulation of sea salt particles and the impact of splashing sea foam. Its intrinsic factor is that the rust layer generated on the surface of steel plays a special role. Hou et al. [9], by simulating the dry-wet cycles in the splash zone, found that the corrosion rate of steel in the splash zone was higher than that in the sea water, mainly due to the increased cathode current caused by the oxidizing effect of the rust layer itself, and the surface rust layer acted as a strong oxidizing agent in the wetting process. In other words, the reduction reaction of $Fe^{3+}$ to $Fe^{2+}$ took place in the rust layer. On the other hand, in the drying process, due to air oxidation, $Fe^{2+}$ in the rust layer was oxidized to $Fe^{3+}$, there were more $Fe_3O_4$ in the rust layer, and at the same time contain different amounts of α-FeOOH, β-FeOOH and γ-FeOOH. The inner rust layer ($Fe_3O_4$) had good electrical conductivity, making the FeOOH in the outer rust layer easy to be reduced, thus showing the difference in reducing current between the ocean water and the ocean spray splashing area.

In the field, organic coating is mostly used to protect atmospheric area and splash area, and sacrificial anode + coating is mostly used to protect tidal range area, full immersion area and sea mud area. Compared with the atmospheric area, the splash area is not only corroded by the marine atmosphere environment, but also affected by the dry-wet cycles, under these circumstances that water molecules may diffuse in the coating, causing the deterioration of the coating and aggravating the corrosion of the metal under the coating [10,11].

Metal thermal spraying aluminum, zinc and their alloys is an effective method to protect steel structures in splash zone. Metal thermal spraying layer has outstanding anti-corrosion performance in marine environment, can shield the corrosion of steel by water, air and other corrosive media, and can act as a sacrificial anode. In addition, the dense oxide film formed on the surface of metal particles in the coating also plays an anti-corrosion role [12].

Bohai ocean in China belongs to low salt sea waters, only for 10 to 20 psu salinity. This article in view of the Bohai Marine splash area, analyzed the corrosion behavior of four kinds of coating metal (Al, Mg, Cu and Zn) in the dry-wet cycles and low concentration of chlorine ion. This paper provides a reference for metal anti-corrosion in marine dry-wet cycles.

## 2. EXPERIMENTAL SETTINGS

(1) Electroplating process. The D32 sample was successively pre-treated by acetone and deionized water, and then dried in a vacuum dryer for 24 h. Before the electroplating experiment, waterproof sandpaper #800~#1200 was used to grind the surface step by step until no obvious scratches were found on the surface, and then the polishing process was carried out. The traditional two-electrode electroplating system was adopted in the experiment, in which the anode was 99.99% metal electrode and the cathode was D32 steel (25×25×2 $mm^3$, main components as shown in Tab.1). The solution with the concentration of 1 mol/L was prepared by corresponding chloride salt, in which the EMIC (1- methyl -3 - ethyl imidazole chloride) -$AlCl_3$ solution [13] was for Al electroplating, the $CH_3MgCl$/THF (Tetrahydrofuran) solution [14] was for Mg electroplating, $C_6H_5K_3O_7/C_2H_8N_2/H_3BO_3/CuCl_2$ solution [15] was for Cu electroplating and the $ZnCl_2$ solution [16] was for Zn electroplating. The distance between the sample and the anode was adjusted to 6 cm, and the surface of the two electrodes was ensured to be in alignment. The electroplating current density was 6 $A/dm^2$, the temperature was at a constant 50℃, the stirring speed of magnetic rotor was 200 r/min, the duty cycle was 40%, and the frequency was 50 Hz. The electroplating time was 30 min, and the final coating thickness was 30±1 μm.

**Table 1.** Main composition of D32 steel (wt.%)

| C | Si | Mn | P | S | Cr | Mo | Ni | Cu | Al | V | Ti | Fe |
|---|---|---|---|---|---|---|---|---|---|---|---|---|
| 0.14 | 0.36 | 1.38 | 0.018 | 0.013 | 0.01 | 0.01 | 0.02 | 0.03 | 0.033 | 0.001 | 0.018 | Ceq |

(2) Experimental solution. The analytical pure NaCl and deionized water were used to prepare the experimental solution with a mass fraction of 2% (2 wt.% NaCl solution) to simulate the low salinity marine environment. After the NaCl in solution was completely dissolved at 50℃, it was left standing at room temperature for 24 h to ensure that no solid particles were precipitated.

(3) Dry-wet cycle experiment. Five drops of experimental solution were dropped on the electroplated D32 sample to ensure that the surface of the sample was wetted by the experimental solution, and then the sample was dried naturally in the air (the room temperature was controlled at 20℃). After exposed for 12 h (the experimental solution evaporated completely), the experimental solution was dropped again and repeated operation (lasting for 10 days) was performed to simulate the dry-wet cycles.

(4) Electrochemical experiment settings. Three-electrode electrochemical testing system was adopted for the electrochemical tests, in which the working electrode (WE) was five samples, including Cu-, Mg-, Zn-, Al-coated D32 steel and pure D32 steel, the auxiliary electrode (AE) was Pt electrode, and reference electrode (RE) was SCE (saturated calomel electrode). Reference electrode was contacted with solution through Luggin capillary, and the distance of the Luggin capillary tip and five samples was less than 2 mm, thus to ignore the IR drop of solution. The workstation used for electrochemical test was PARSTAT 2273, in which the scanning rate of polarization curve was set as

0.3 mV/s, and the scanning potential range was ±250 mV (relative to open circuit potential, $E_{OCP}$). The scanning range of electrochemical impedance spectrum (EIS) was $10^5$-$10^{-2}$ Hz, and the amplitude was 5 mV.

It should be noted that when the fluctuation of open circuit potential was less than ±5 mV within 300 s, the whole system was considered to be in a stable state, therefore under this condition the EIS curve and polarization curve can be tested. All tests were carried out at a constant temperature of 20℃.

Data processing: Electrochemical data processing adopted the software "PowerSuite" and "ZSimpWin" of the system. The fitted error of EIS curves was controlled in $10^{-4}$.

(5) Macro corrosion data analysis. The corrosion resistance of different coatings was analyzed by immersion tests. The dry-wet cycle test was set as described above, and every 12 h was a test cycle. After 30 days of the test, the corrosion products on the surface were removed by standard rust remover (500 mL hydrochloric acid + 500 mL deionized water + 3.5 g hexamethylenetetramine), and the maximum corrosion pit depth on the surface and corrosion morphology were tested by 3D scanning microscope, and then the general corrosion rate (Eq.1) and pitting corrosion rate (Eq.2) were calculated.

$$v_1 = 87600 \times \frac{\Delta G}{S \times t \times \rho} \quad (1)$$

Where, $v_1$ was general corrosion rate in mm/a, $\triangle G$ was the weight loss in g, $S$ was surface area of 1 $cm^2$, $t$ was experimental time in h and $\rho$ was density.

$$v_2 = 87600 \times \frac{H_{max}}{t} \quad (2)$$

Where, $v_2$ was pit corrosion rate in mm/a, $H_{max}$ was the max pit depth obtained by Zeiss Microscope in mm and $t$ was experimental time in h.

## 3. RESULTS AND DISCUSSION

### *3.1 Electrochemical analysis*

Fig.1 showed the test results of polarization curves in dry-wet cycles for five samples (Cu-, Mg-, Zn-, Al-coated D32 steel and pure D32 steel), Tab.2 showed the fitting results of polarization curves and Fig.2 showed the comparison of corrosion potential ($E_{corr}$) and corrosion current density ($I_{corr}$) of different samples. Compared with the pure D32 steel, the $E_{OCP}$ of Zn/Al/Mg-coated steel was more negative, which was -0.886 V, -0.947 V and -1.341 V, respectively, while the $E_{OCP}$ of Cu-coated steel was more positive of -0.514 V. According to the polarization curve test results, different metal-coated steels were activated and corroded in Tafel region, and Tafel slope ratios were controlled by anode process. Under the research conditions of this paper, the Zn-coated steel and Cu-coated steel showed lower $I_{corr}$ of 4.97 μA/$cm^2$ and 6.32 μA/$cm^2$, respectively, while the Al-coated steel showed the highest $I_{corr}$ of 19.14 μA/$cm^2$.

In terms of the activity of different metals, Al as a dull metal was still easy to form dense $Al_2O_3$ passivation film in the dry-wet cycles. The $I_{corr}$ of Al-coated steel was the largest among the five samples, which was higher than that of pure D32 steel (15.01 μA/$cm^2$). Under the condition of the

research in this paper, the concentration of chloride ion was only 2%, and the current international Al sacrificial anode and related research results showed that Al under the condition of not less than 3.6% of chlorine salt concentration can keep the activation corrosion state. Therefore, the main reason for the largest $I_{corr}$ of Al-coated steel in this paper was that the ratio of wetting area to drying area gradually changed in the process of natural evaporation of droplets in the air under dry-wet cycles, forming micro-batteries in the passivation film, and the wetting position as the anode gradually destroyed the corrosion product film [17,18]. During 20 dry-wet cycles, the tight surface film cracked, showing an active corrosion state.

For the Cu-coated steel, CuO and $Cu_2O$ were firstly generated. Under the condition of containing chloride ions, $Cu_2O$ dissolved to form $Cu^{2+}$, and finally mainly formed loose corrosion product $Cu_2Cl_2(OH)_3$ by $Cu \rightarrow Cu_2O \rightarrow Cu^{2+} \rightarrow Cu_2Cl_2(OH)_3$ [19]. However, $Cu_2Cl_2(OH)_3$ did not conduct electricity, which showed good electrical insulation, so its corrosion current density was small. Due to its loose structure, it was easy to promote the diffusion of chloride ions and cause pitting.

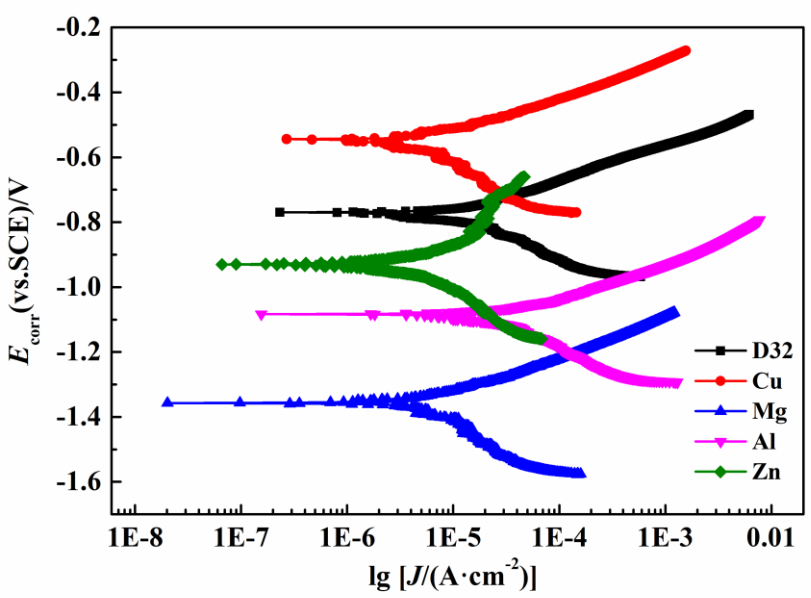


**Figure 1.** Polarization curves of five samples (Cu-, Mg-, Zn-, Al-coated D32 steel and pure D32 steel) in 2 wt.% NaCl solution at 20℃ lasting for 10 days (20 dry-wet cycles)

For the Mg-coated steel, the electronegativity was the lowest, -1.36 V, and the activity was the highest. However, the $I_{corr}$ of the Mg-coated steel was 10.66 μA/cm$^2$, which was lower than that of pure D32 steel and the Al-coated steel, but was higher than that of Zn-coated steel and Cu-coated steel. This was because the corrosion rate of Mg with highest corrosion activity among the five metals was faster at the initial stage, leading to a rapid accumulation of corrosion products on Mg surface. For another aspect, as can be seen from Tafel slope ratio, Mg-coated steel was the largest, indicating that the corrosion process was controlled by cation diffusion process at this time, so the $I_{corr}$ was relatively low [20,21].

For the Zn-coated steel, relevant studies showed that in most natural environments, the corrosion rate of zinc was only 1/10-1/100 of D32 steel. However, in the dry-wet cycles, the results of this study showed that the corrosion rate of Zn-coated steel was 1/3 of that of D32 steel [22]. In addition, where Zn coating was damaged and Fe was exposed, the Zn provided additional protection for Fe due to galvanic interaction [23,24], which was not available for Mg-coated [25] and Al-coated steel [26,27].

**Table 2.** Fitting results of polarization curves of five samples (Cu-, Mg-, Zn-, Al-coated D32 steel and pure D32 steel) in 2 wt.% NaCl solution at 20℃ lasting for 10 days (20 dry-wet cycles)

| Element | $E_{corr}$ (Vvs.SCE) | $I_{corr}$ (μA/cm$^2$) | $\beta_a$ (mV/dec) | $\beta_c$ (mV/dec) | $r=\beta_a/\beta_c$ |
|---|---|---|---|---|---|
| D32 | -0.774 | 15.01 | 178 | 120 | 1.48 |
| Cu | -0.557 | 6.32 | 281 | 98 | 2.87 |
| Mg | -1.363 | 10.66 | 455 | 144 | 3.17 |
| Al | -1.085 | 19.14 | 128 | 56 | 2.29 |
| Zn | -0.937 | 4.97 | 205 | 149 | 1.37 |

Fig.2 showed the EIS results of different metal-coated samples in dry-wet cycles, and Fig.3 showed the fitting parameter comparison of different metal-coated samples.

It can be seen from the Bode plots (log*f*-*φ* curve) of the different metal-coated samples in dry-wet cycles, the curves all showed two peak values, indicating that there were two time constants [28]. Considering the electrochemical corrosion process, the equivalent circuit was chosen as $R_s(Q(R_{p(}C_{dl}R_{ct})))$, in which $R_s$ was the solution resistance, $Q$ was the system capacitance, $R_p$ was the polarization resistance, $C_{dl}$ was the double layer capacitance, and $R_{ct}$ was the charge transfer resistance.

In the Nyquist diagrams, the reactance arc radius showed Al>Cu>Zn>Mg-coated steels, and the Nyquist diagrams of Zn-coated steel and pure D32 steel basically coincided, while the Nyquist diagrams of Zn-coated steel [29], D32 steel and Mg-coated steel [30] basically coincide in the high frequency regions. As can be seen from the fitting parameters of EIS curves, the polarization resistance of Al-coated steel was the largest ($R_p$ = 7040.17 Ω·cm$^2$), and its charge transfer resistance ($R_{ct}$) was much smaller than that of Cu-coated steel, which was close to that of Zn-coated steel and pure D32 steel. This was because although Al was easy to generate dense passivation film with a larger $R_p$, pitting corrosion caused in dry-wet cycles also promoted the activation process of the metal itself, showing a smaller $R_{ct}$ [31].

Among the five metal-coated samples, the largest double layer capacitance ($C_{dl}$ = 1.19×10$^{-3}$ F/cm$^2$) and the lowest charge transfer resistance ($R_{ct}$ = 2.88×10$^3$ Ω·cm$^2$) of Mg-coated steel were obtained due to its highest electrochemical activity, while the polarization resistance ($R_p$ = 95.77 Ω·cm$^2$) was much smaller than that of Al-coated steel and slightly larger than the other three metal-coated steels. From the point of view of the electrochemical reaction process, among the five metal-coated steels mentioned above, the Cu-coated steel had the largest charge transfer resistance ($R_{ct}$ = 1.43×10$^4$ Ω·cm$^2$) [32], indicating a largest corrosion resistance, because the Cu corrosion products

was non-conductive to hinder the electron transfer process, thus inhibiting the corrosion reaction process.

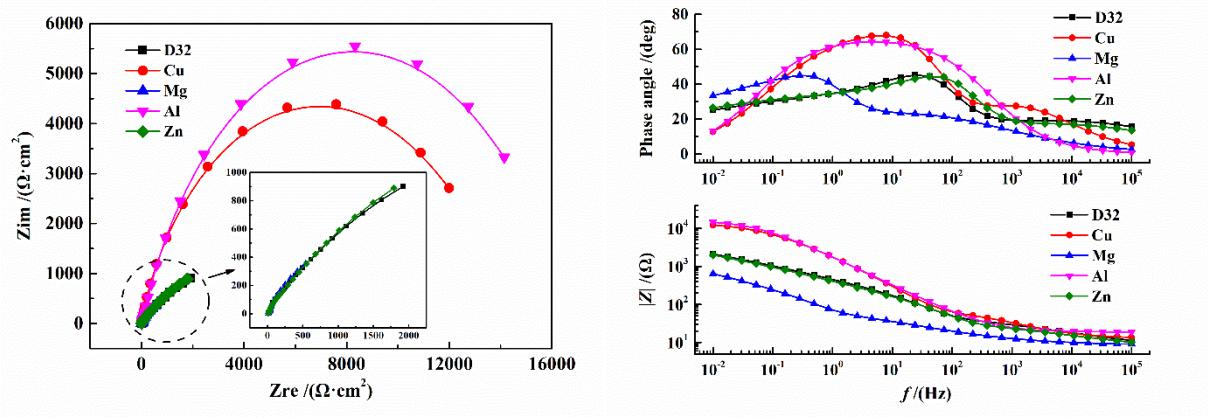


(a) Nyquist diagrams (b) Bode plots

**Figure 2.** EIS curves of five samples (Cu-, Mg-, Zn-, Al-coated D32 steel and pure D32 steel) in 2 wt.% NaCl solution at 20℃ lasting for 10 days (20 dry-wet cycles)

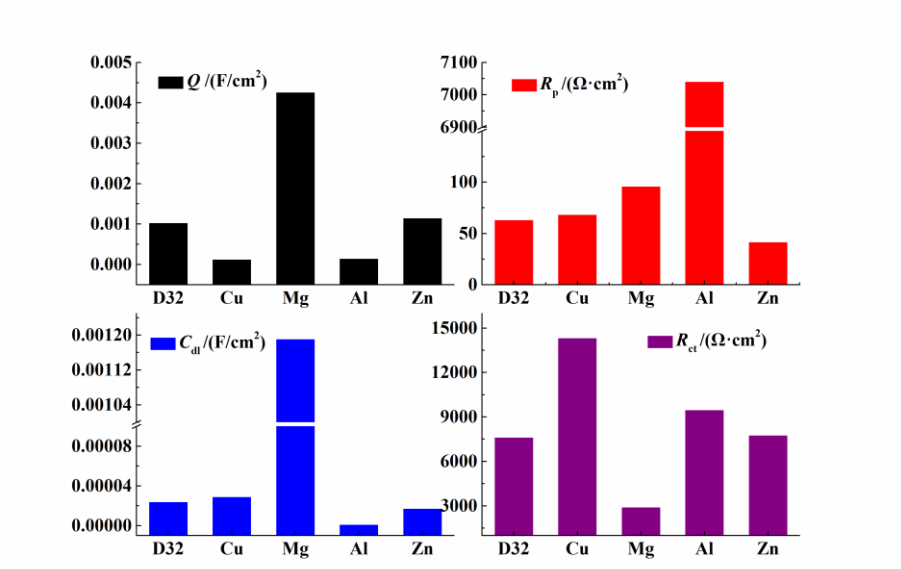


**Figure 3.** Fitted results of EIS curves of five samples (Cu-, Mg-, Zn-, Al-coated D32 steel and pure D32 steel) in 2 wt.% NaCl solution at 20℃ lasting for 10 days (20 dry-wet cycles)

### *3.2 Corrosion rate and corrosion morphology*

The immersion for 30-day dry-wet cycle test was carried out. After the test, the surface corrosion products were removed, the general corrosion rate was calculated, and the maximum corrosion pit depth on the surface was tested by 3D scanning microscope. The results were shown in Fig.4 and Fig.5.

In terms of general corrosion rate, Mg>Zn>Cu>Al-coated steel, which was because corrosion activity of Mg was the highest among the five metal-coated steels, so its general corrosion rate was the highest, while a dense corrosion product film of Al was formed on its surface, which hindered the general corrosion process due to its passivation characteristics [33,34]. However, the pitting corrosion rate results showed Al>Cu>Zn>Mg-coated steel. This was because the dense passivation film was formed on the surface of the Al-coated steel, and obvious pitting behavior occurred under the condition of dry-wet cycles and low chloride ion concentration. Therefore, the pitting corrosion rate of Al-coated steel was the highest among the five samples. For the Cu-coated steel, on the one hand, the Cu corrosion products showed good electrical insulation, and the loose corrosion product layer easily absorbed chloride ions, which caused the pitting phenomenon of the matrix [35].

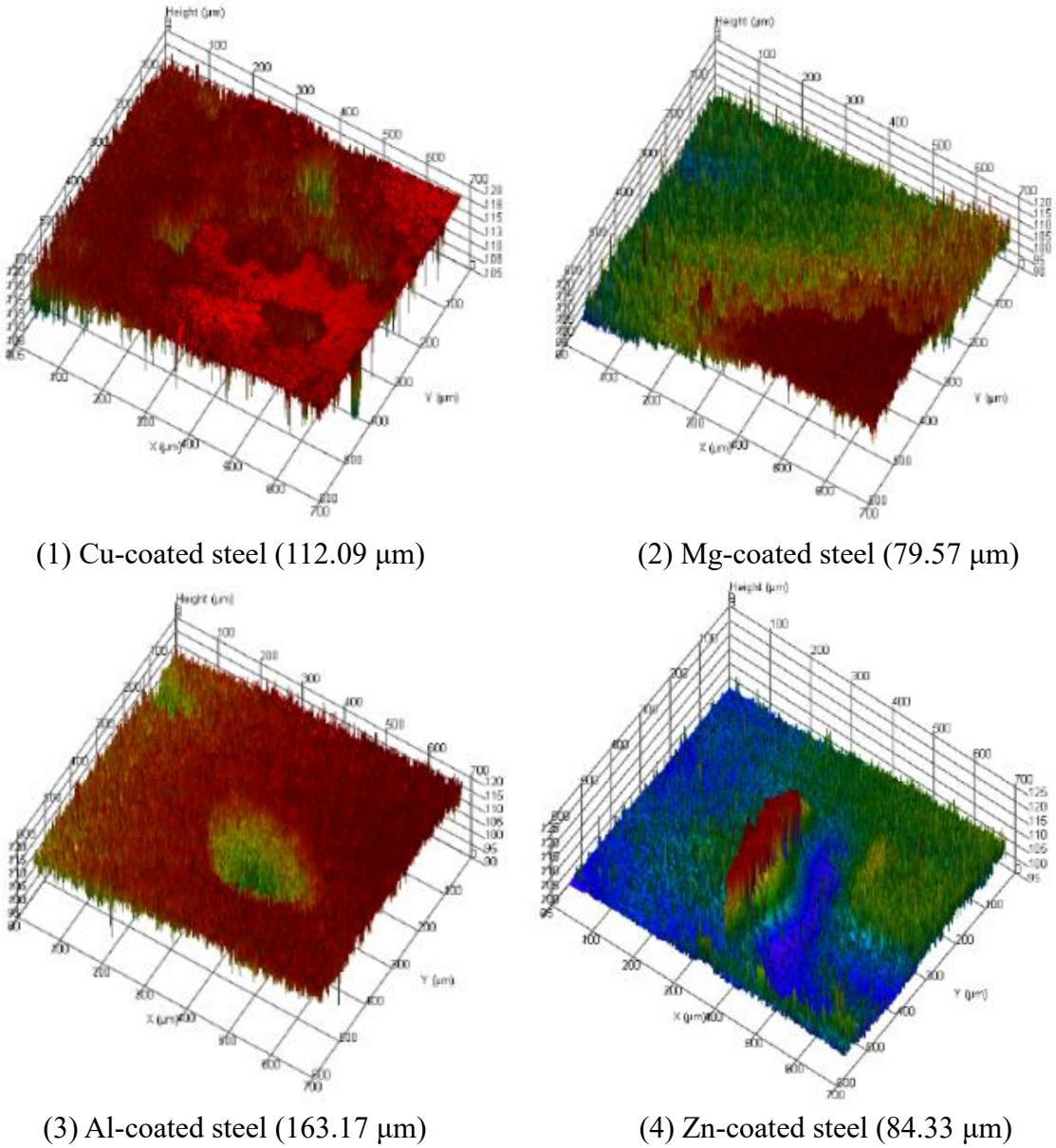

(1) Cu-coated steel (112.09 μm) (2) Mg-coated steel (79.57 μm)

(3) Al-coated steel (163.17 μm) (4) Zn-coated steel (84.33 μm)

**Figure 4.** Pitting morphology and maximum pitting depth of five samples (Cu-, Mg-, Zn-, Al-coated D32 steel and pure D32 steel) in 2 wt.% NaCl solution at 20℃ lasting for 60 dry-wet cycles

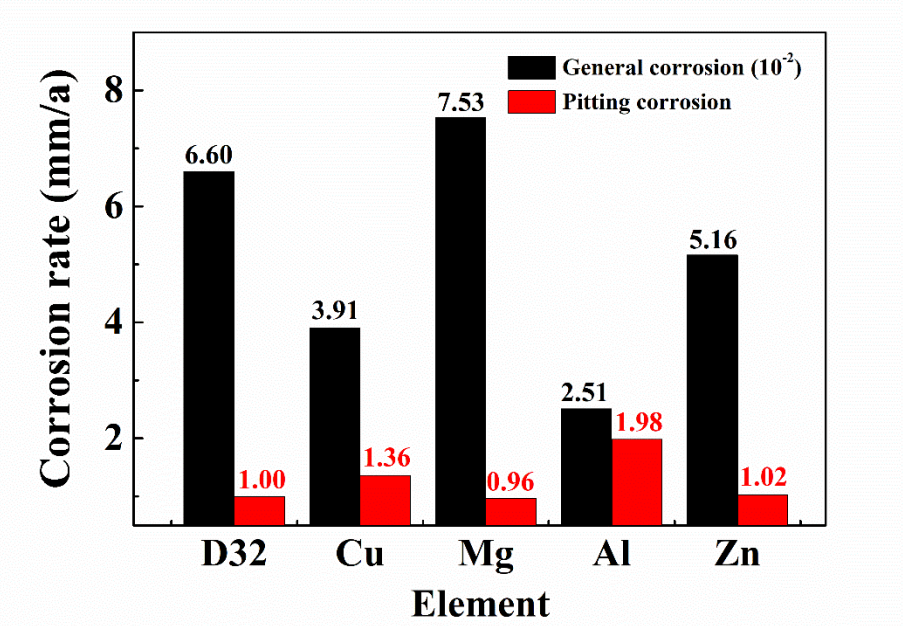


**Figure 5.** General corrosion rate and pitting corrosion rate of five samples (Cu-, Mg-, Zn-, Al-coated D32 steel and pure D32 steel) in 2 wt.% NaCl solution at 20℃ lasting for 60 dry-wet cycles

On the other hand, due to the positive potential of Cu, Cu-Fe galvanic corrosion promoted the pitting corrosion process while the Cu-layer was damaged. For D32, Mg- and Zn-coated steels, they exhibited active corrosion state under dry-wet cycles and chloride ion environment. Therefore, the pitting corrosion rates of the three samples were basically the same (Mg-coated steel 0.96 mm/a [36], Zn-coated steel 1.02 mm/a [37] and D32 steel 1.00 mm/a) under the experimental conditions in this paper.

## 4. CONCLUSIONS

In this paper, the corrosion characteristics of five metal-coated samples in low chloride ion and dry-wet cycles were analyzed to determine the best metal coatings for D32 steel in ocean splash environment, and the main conclusions were as follows:

(1) The electrochemical test results showed that under the condition of dry-wet cycles (10 days, 20 cycles) and low chloride ion concentration (2% by mass fraction), all the five metal-coated steels showed active corrosion state and were in anodic control state. The corrosion potential of five metal-coated samples showed that Cu<Zn<Al<Mg-coated steels, while the corrosion current density indicated Zn<Cu<Mg<Al-coated samples. At the same time, compared with Al-coated and Mg-coated steel, the corrosion products on the surface of Cu-coated steel had electrical insulation, and Zn-coated steel can provide cathodic protection, so it can be used in the ocean splash environment.

(2) The corrosion morphology of the five samples was analyzed through 60 dry-wet cycles, and the general corrosion rate was as follows: Al<Cu<Zn<Mg-coated steels, while the pitting corrosion rate was Mg<Zn<Cu<Al-coated steels.

In consideration of the pitting corrosion process of the five samples, the failure process will be greatly accelerated while the metal coating was damaged especially for the Cu, and the Zn-coated steel can provide the cathodic protection. On the whole, the Zn-coated method can be used to protect D32 steel in the low-salinity dry-wet cycles in the splash ocean.

## References


1. X.R. Zhu, G.Q. Huang, L.Y. Lin and D.Y. Liu, *Corros. Eng. Sci. Techn.*, 43 (2008) 328.
2. C. Thee, L. Hao, J. Dong, M. Xin, W. Xin and X Li, *Corros. Sci.*, 78 (2014) 130.
3. R. Jeffrey and R.E. Melchers, *Corrosion*, 65 (2009) 695.
4. R.E. Melchers, *Corros. Sci.*, 81 (2014) 110.
5. A. Aghajani, *Mater. Performance*, 47 (2008) 38.
6. H. Meng, X. Hu and A. Neville, *Wear*, 263 (2007) 355.
7. K.M. Anwar Hossain, S.M. Easa and M. Lachemi, *Build. Environ.*, 44 (2009) 713.
8. X.R. Zhu, G.Q. Huang and C.F. Ling, *Chin. Jour. Oceanol. Limn.*, 15 (1997) 378.
9. B.R. Hou and B. Xiang, *B. Mater. Sci.*, 26 (2003) 307.
10. K. Gong, M. Wu, F. Xie, G. Liu and D. Sun, *Constr. Build. Mater.*, 260 (2020) 120478.
11. C. Yang, X. Xing, Z.L. Li and S.X. Zhang, *Polymers-basel*, 12 (2020) 138.
12. B.R. Hou, J.Z. Duan, Y. Li and J.L. Zhang, *Corros. Eng. Sci. Techn.*, 38 (2003) 157.
13. M.R. Ali, A.P. Abbott, K.S. Ryder, *J. Electrochem.*, 21 (2015) 172.
14. R.J. Gummow, Y.H. He, *J. Electrochem. Soc.*, 157 (2010) E45.
15. W.Q. Li, L. Jin, J.Q. Yang, Z.Y. Wang, F.Z. Yang, D.P. Zhan and Z.Q. Tian, *Chem. J. Chinese U.*, 42 (2021) 2919.
16. F. Jamalif, I. Danaee and D. Zaaei, *Mater. Corros.*, 66 (2015) 459.
17. L.L. Fan, Y. Li, X.Y. Zhao, Y.X. Yu, C.G. Zhou and J.B. Sha, *Corros. Sci.*, 192 (2021) 109811.
18. S.H. Lei, S. Wang, H. Zhong, X. Ma and Z.F. Cao, *Surf. Coat. Tech.*, 419 (2021) 127290.
19. Y. Liu, J.J. Yang, H. Yang, K.M Li, Y.T. Qiu, W.C. Zhang and S.F. Zhou, *Surf. Coat. Tech.*, 428 (2021) 127868.
20. J.L. Davies, C.F. Glover, J. Van de Langkruis, E. Zoestbergen and G. Williams, *Corros. Sci.*, 100 (2015) 607.
21. G.D. Park, J.H. Yang, K.H. Lee, H.J. Kim, S.H. Lee, J. Kang, Y.S. Yun and M.H. Lee, *Corros. Sci.*, 192 (2021) 109829.
22. Y. Deo, R. Ghosh, A. Nag, D.V. Kumar, R. Mondal and A. Banerjee, *Electrochim. Acta*, 399 (2021) 139379.
23. J.H. Kang, K. Doyub, K.D. Hwi and K. Sung-Joon, *Surf. Coat. Tech.*, 357 (2019) 1069.
24. K. Wang, B. Zhu, Z. Wang, Y. Liu and S. Li, *Surf. Coat. Tech.*, 380 (2019) 1.
25. S.J. Pan, W.T. Tsai and I.W. Sun, *Electrochem. Solid St.*, 13 (2010) D69.
26. M.R. Ali, A. Nishikata, T. Tsuru, *Electroanal. Chem.*, 513 (2001) 111.
27. Y. Zheng, S. Zhang, X. Lu, Q. Wang, Y. Zuo and L. Liu, *Chinese J. Chem. Eng.*, 20 (2012) 130.
28. H. Li, Y.J. Qiang, W.J. Zhao and S.T. Zhang, *Corros. Sci.*, 191 (2021) 109715.
29. K.S. Jyotheender, M.K.P. Kumar and C. Srivastava, *Surf. Coat. Tech.*, 423 (2021) 127594.
30. Y. Zhou, P. Zhang and F. Yan, *Mater. Lett.*, 284 (2021) 128930.
31. K.R. Liu, Q. Liu, Q. Han and G.F. Tu, *T. Nonferr. Metal. Soc.*, 21 (2011) 2104.
32. X.X. Zhang, T. Zhang, Y. Lv, Y.P. Zhang, X.Q. Lu, J.Y. Xiao, C. Ma, Z. Li, Z.H. Dong, *Appl. Surf. Sci.*, 569 (2021) 150932.
33. T. Jiang, M.J.C. Brym, G. Dubé, A. Lasia and G.M. Brisard, *Surf. Coat. Tech.*, 201 (2006) 1.
34. J.K. Chang, I.W. Sun, S.J. Pan, M.H. Chuang, M.J. Deng, W.T. Tsai, *T. I. Met. Finish.*, 86 (2008) 227.

35. Y.C. Liang, H.Q. Chu, M.Z. Guo, Y.X. Zeng, Z.Y. Zhu and L.H. Jiang, *Constr. Build. Mater.*, 304 (2021) 124605.
36. X. Wang, C. Jing, Y.X. Chen, X.S. Wang, G. Zhao, X. Zhang, L. Wu, X.Y. Liu, B.Q. Dong, Y.X. Zhang, *J. Magnes. Alloy.*, 8 (2020) 291.
37. H.L.Yao, X.Z. Hu, Z.H. Yi, J. Xia, X.Y. Tu, S.B. Li, B. Yu, M.X. Zhang, X.B. Bai, Q.Y. Chen, H.T. Wang, *Surf. Coat. Tech.*, 422 (2021) 127557.